Magnetically-Induced Optical Transparency on a Forbidden Transition in Strontium for Cavity-Enhanced Spectroscopy

by

Matthew N. Winchester

Thesis defense date

April 6$^{\text{th}}$, 2017

Thesis advisor: Prof. James K. Thompson

Department of Physics

Honors Council representative: Prof. Paul Beale

Department of Physics

Third reader: Inst. Brian Zaharatos

Dept. of Applied Mathematics

Winchester, Matthew N.

Magnetically-Induced Optical Transparency on a Forbidden Transition in Strontium for Cavity-Enhanced Spectroscopy

Thesis directed by Prof. James K. Thompson

In this thesis I describe the generation of a narrow spectroscopic feature using a new technique called "magnetically-induced optical transparency" (MIT). A cold ensemble of ^{88}Sr atoms interacts with a single mode of a high-finesse optical cavity via the 7.5 kHz linewidth, spin forbidden $^1S_0$ to $^3P_1$ transition. By applying a magnetic field that shifts two excited state Zeeman levels, a transmission window is opened through the cavity where the collective vacuum Rabi splitting due to a single level would normally create destructive interference for probe transmission.

The spectroscopic feature approaches the atomic transition linewidth, which is much narrower than the cavity linewidth, and is highly immune to the reference cavity length fluctuations that limit current state-of-the-art laser frequency stability.

Dedication

For my family.

Acknowledgements

I had an incredible time at JILA and the University of Colorado thanks to my supporting community of family, friends, and coworkers.

Thank you James, for not only being an excellent research advisor, but also for your patience, support, and mentoring throughout my time in the lab.

I would also like to thank the rest of the Thompson lab, specifically Matt, Julia, Graham, Baochen, Denton, Kevin, and Josh. You all made working in the lab something that I would always look forward to.

Thank you Mom and Dad, for the love and support, and for always encouraging me to ask questions. Thank you Michael and Joseph for all the laughs.

Contents

Chapter

Tables

Table

Figures

Figure

Chapter 1

Introduction

1.1 Background and context

In recent years there has been a push within the physics community to engineer and control quantum systems, especially using the tools of atomic physics. Studying the interactions between atoms and light not only leads to a deeper understanding of fundamental physics, but also provides many applications in precision measurement sensing technologies.

The canonical example of a modern precision measurement technology which harnesses the quantum nature of atoms and light is the atomic clock. Atomic clocks define the most precise time and frequency standards in human history, and work by measuring the frequency of an atomic transition. The SI second is currently defined as "the duration of 9,192,631,770 periods of the radiation corresponding to the transition between the two hyperfine levels of the ground state of the ^{133} Cs atom" [1].

The transition frequencies of atomic clocks are probed using another precision measurement technology: the laser. Lasers provide a spatially and temporally coherent source of electromagnetic radiation by relying on the process of stimulated emission. In order to accurately measure the transition frequencies of atomic clocks, the probe lasers must be very precise themselves, emitting only a narrow frequency band of radiation which is used to drive transitions.

1.2 Applications

There has been a dedicated effort to improve the frequency stability of lasers [2] used to probe optical atomic clocks [3, 4, 5]. Improvements in these precision measurement systems have many applications, some of which are briefly described below.

1.2.1 Quantum sensing

Atomic clocks rely on the precise measurement of an optical transition frequency to define a time standard. These transition frequencies can be measured so well that incredibly small perturbations (from electric/magnetic fields, gravity, etc.) which shift the transition frequency can be accurately resolved. This means that atomic clocks can be used as extremely precise sensors. For example, atomic clocks can be used in relativistic geodesy studies to precisely measure local gravitational field strength. Current atomic clocks are so sensitive that they can resolve height differences of less than a meter [6].

1.2.2 Fundamental physics

Improvements in these precision measurement technologies are also essential for advancing a broad range of scientific pursuits such as searching for variations in fundamental constants [7], gravitational wave detection [8, 9], and physics beyond the standard model [10, 11]. Although perturbations from these sources may be incredibly small, atomic clocks are reaching the precision and time stability needed to resolve these effects.

1.2.3 Synchronized devices

In addition to scientific advances, improvements in precision measurement would also lead to many useful technological advances. Any network of interacting devices which require time sensitive communication needs to be synchronized to a stable clock. The global positioning system (GPS) is one example of a technology that would benefit from improvements in clock precision. GPS satellites

continuously transmit their current time and orbital parameters (each carry a synchronized cesium atomic clock on board). By computing the positions of multiple satellites (at least 4) based on this information, GPS receivers on Earth can determine the user's location. Improvements in atomic clock precision and synchronization would result in more sensitive GPS positioning [12].

1.3 Improving precision measurement limits

A variety of both active and passive methods exist for frequency stabilizing lasers. One widely used method is the Pound-Drever-Hall locking technique, which uses a stable optical cavity as a frequency reference for the laser to follow.

The frequency stability of current state-of-the-art lasers used to probe atomic clocks is limited by thermal fluctuations in the reference cavity mirror coatings, substrates, and spacer [13]. This problem can be alleviated by creating systems that rely on an ensemble of atoms, rather than the reference cavity, to achieve stable optical coherence. Recent approaches include cavity-assisted non-linear spectroscopy [14, 15, 16] and superradiant lasers [17, 18, 19, 20]. Both approaches use narrow forbidden transitions with linewidths ranging from 7.5 kHz to 1 mHz. These novel systems are absolute frequency references and are intrinsically less sensitive to both fundamental thermal and technical vibrations that create noise on the optical cavity's resonance frequency.

This thesis describes a novel spectroscopy technique in which a static magnetic field can induce optical transparency in the transmission spectrum of an optical cavity. Important metrics of a frequency reference, such as linewidth and sensitivity to the cavity, are experimentally measured for the frequency discriminator generated with this technique. The center frequency of the transparency window is shown to be insensitive to changes in the cavity-resonance frequency, which limit the precision of today's best lasers, and approaches the natural linewidth of the 7.5 kHz optical transition.

1.4 Comparison to electromagnetically induced transparency (EIT)

Electromagnetically induced transparency (EIT) is a well–studied optical effect where a coherent interference between quantum states creates a narrow transparency window through an opaque absorption line [21, 22, 23].

In analogy to EIT, we refer to the effect studied in this thesis as magnetically induced transparency (MIT). In EIT, a control laser is used to create a variable-width transparency window for slowing light [24], for stopping light [25], for quantum memories [26], and even for creating effective photon-photon interactions [27, 28, 29]. It might be possible to utilize controlled magnetic fields and long-lived optical states to realize similar goals.

1.5 Thesis overview

This thesis is organized as follows: Chapter 2 provides a brief review of spin–$\frac{1}{2}$ systems and quantum harmonic oscillators, then gives an in–depth description of several cavity quantum electrodynamics (cavity QED) systems. The Jaynes–Cummings and Tavis–Cummings Hamiltonians describing one or many two–level atoms coupled to a single mode of an optical cavity are discussed and then generalized to describe multi–level atoms coupled to a cavity. Chapter 3 gives an overview of the experiment apparatus, as well as atom trapping and cooling techniques. Chapter 4 provides experimental results and data analysis. Finally, Chapter 5 contains last remarks and conclusions about this work.

Chapter 2

Background and Theory

2.1 Overview

The prototypical system studied in cavity quantum electrodynamics (cavity QED) is a single two–level atom coupled to a single mode of an optical cavity. In this chapter I will begin by providing a brief overview of spin–$\frac{1}{2}$ systems and quantum harmonic oscillators, which are accurate models of two–level atoms and cavity modes respectively. I will then discuss the Jaynes–Cummings Hamiltonian, which describes the dynamics of an atom coupled to an optical cavity mode, followed by the Tavis–Cummings Hamiltonian, which describes many atoms coupled to an optical cavity mode. Lastly I will generalize the Tavis–Cummings Hamiltonian to include two–level atoms, which describes the cavity QED system used in this work.

2.2 Spin–$\frac{1}{2}$ systems

Spin $\boldsymbol{S}$ is an intrinsic form of angular momentum and a unique property of quantum mechanical particles. All particles have either an integer or half–integer spin, and the spin projection along a quantization axis $\boldsymbol{q}$ can take a value ranging from $m_s = -S, -S+1, ..., S-1, S$. The simplest case considered here is the spin–$\frac{1}{2}$ system, where the spin projection measured along any axis is either $m_s = +1/2$ ("spin up") or $m_s = -1/2$ ("spin down"). The most general quantum state of a spin–$\frac{1}{2}$ system is a superposition of the spin–up and spin–down states:

$$|\psi\rangle = \cos\frac{\theta}{2}|0\rangle + e^{\imath\phi}\sin\frac{\theta}{2}|1\rangle \tag{2.1}$$

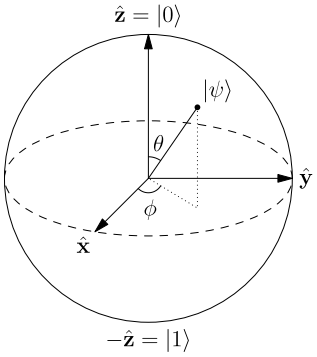

(a) Any two–level quantum system, including spin–$\frac{1}{2}$ particles and two–level atoms, can be represented as a vector pointing to the surface of the Bloch sphere (image adapted from Glosser.ca, 2012).

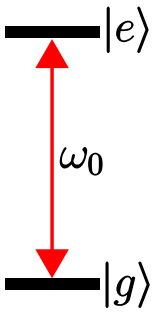

(b) Two–level atom with transition frequency ω_0

Figure 2.1: Two–level quantum systems.

where $|0\rangle$ is the spin up state and $|1\rangle$ is the spin down state (for quantization axis $\boldsymbol{q}$ along $\hat{\boldsymbol{z}}$). The spin up and spin down states are orthonormal and form a complete basis:

$$\langle g|e\rangle = \delta_{eg} \tag{2.2}$$

The general quantum state of equation 2.1 can be visualized as a vector with unit magnitude pointing to the surface of the "Bloch" sphere (see Figure 2.1a).

The most general observable of the spin–$\frac{1}{2}$ system is a linear combination of the three Pauli operators, which correspond to measuring the spin projection of the particle along the $\boldsymbol{x}$, $\boldsymbol{y}$, and $\boldsymbol{z}$ axes respectively:

$$\hat{\sigma}_X = \begin{pmatrix} 0 & 1 \\ 1 & 0 \end{pmatrix}; \quad \hat{\sigma}_Y = \begin{pmatrix} 0 & -\imath \\ \imath & 0 \end{pmatrix}; \quad \hat{\sigma}_Z = \begin{pmatrix} 1 & 0 \\ 0 & -1 \end{pmatrix} \tag{2.3}$$

This spin–$\frac{1}{2}$ formalism is much more general. The most simple model of an atom has a single ground state $|g\rangle$ and a single excited state $|e\rangle$, separated in energy by $\Delta E = \hbar\omega_0$ (see Figure 2.1). Although atoms have many possible transitions, a two–level approximation is valid when all other transitions are far off-resonance. In this case, the atom system can be mapped onto the spin–$\frac{1}{2}$

system by simply making the substitutions $|1\rangle \rightarrow |g\rangle$ and $|0\rangle \rightarrow |e\rangle$. If we set the average energy of the two states to zero, the atom Hamiltonian takes the form:

$$\hat{H}_a = \hbar\omega_0 \frac{\hat{\sigma}_Z}{2} \tag{2.4}$$

It will also be useful for following sections of this chapter to introduce the atomic raising and lowering operators here:

$$\hat{\sigma}_\pm = \frac{1}{2}(\hat{\sigma}_X \pm \imath\hat{\sigma}_Y) \tag{2.5}$$

These projection operators can also be written in terms of the spin–$\frac{1}{2}$ eigenstates:

$$\hat{\sigma}_+ = |e\rangle\langle g|\,; \quad \hat{\sigma}_- = |g\rangle\langle e| \tag{2.6}$$

The raising operator brings an atom from the ground state up to the excited state, while the lowering operator brings an atom from the excited state down to the ground state (see Figure 2.2):

$$\hat{\sigma}_+ |g\rangle = |e\rangle\,; \quad \hat{\sigma}_- |e\rangle = |g\rangle \tag{2.7}$$

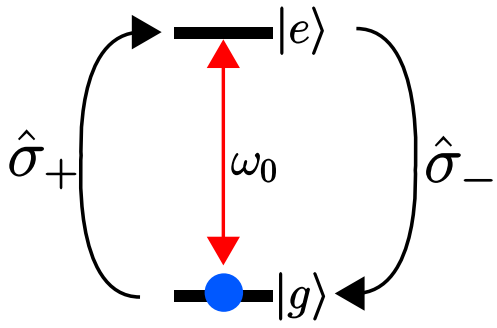

Figure 2.2: Action of raising and lowering operators on a two–level atom.

With this simple model of an atom as a two level quantum system, we have learned about half of the players in our cavity QED system. The next section describes the other half: quantum harmonic oscillators.

2.3 Quantum harmonic oscillators

In one dimension, the Hamiltonian of a particle of mass m in a quadratic potential $V(x) = m\omega^2 x^2/2$ is given by:

$$\hat{H} = \frac{\hat{P}^2}{2m} + \frac{m\omega^2 \hat{X}^2}{2} \tag{2.8}$$

where $\hat{P}$ is the particle's momentum and $\hat{X}$ is the particle's position.

If we introduce dimensionless units $x_0 = \sqrt{\hbar/2m\omega}$ and $p_0 = \sqrt{m\omega\hbar/2}$, along with dimensionless operators $\hat{X}_0 = \hat{X}/2x_0$ and $\hat{P}_0 = \hat{P}/2p_0$, the Hamiltonian can be rewritten as:

$$\hat{H} = \hbar\omega(\hat{X}_0^2 + \hat{P}_0^2) \tag{2.9}$$

If we introduce the new "ladder" operators $\hat{a} \equiv \hat{X}_0 + \imath\hat{P}_0$ and $\hat{a}^\dagger \equiv \hat{X}_0 - \imath\hat{P}_0$, we can rewrite the Hamiltonian one last time in the form:

$$\hat{H} = \hbar\omega(\hat{a}^\dagger\hat{a} + 1/2) \tag{2.10}$$

The Hilbert space of this Hamiltonian is spanned by an orthonormal set of "Fock" states, $|n\rangle$. The ladder operators have a simple effect on these states: the creation operator $\hat{a}^\dagger$ brings the system from the $|n\rangle$ state to the $|n+1\rangle$ state, while the annihilation operator $\hat{a}$ lowers the $|n\rangle$ state to the $|n-1\rangle$ state. The following relations must hold for the states to stay normalized:

$$\hat{a}^\dagger|n\rangle = \sqrt{n+1}\,|n+1\rangle\,; \quad \hat{a}\,|n\rangle = \sqrt{n}\,|n-1\rangle \tag{2.11}$$

If we define the number operator $\hat{N}$ as $\hat{N} \equiv \hat{a}^\dagger\hat{a}$, then we also have the relation $\hat{N}\,|n\rangle = n\,|n\rangle$. Using the number operator, it is clear that the Fock states are the energy eigenstates of the Hamiltonian. Each Fock state $|n\rangle$ has energy eigenvalue $E = n\hbar\omega$ (neglecting the $\hbar\omega/2$ zero–point energy offset). Figure 2.3 shows a pictorial representation of the energy spectrum of the quantum harmonic oscillator, as well as the actions of the creation and annihilation operators on the energy eigenstates.

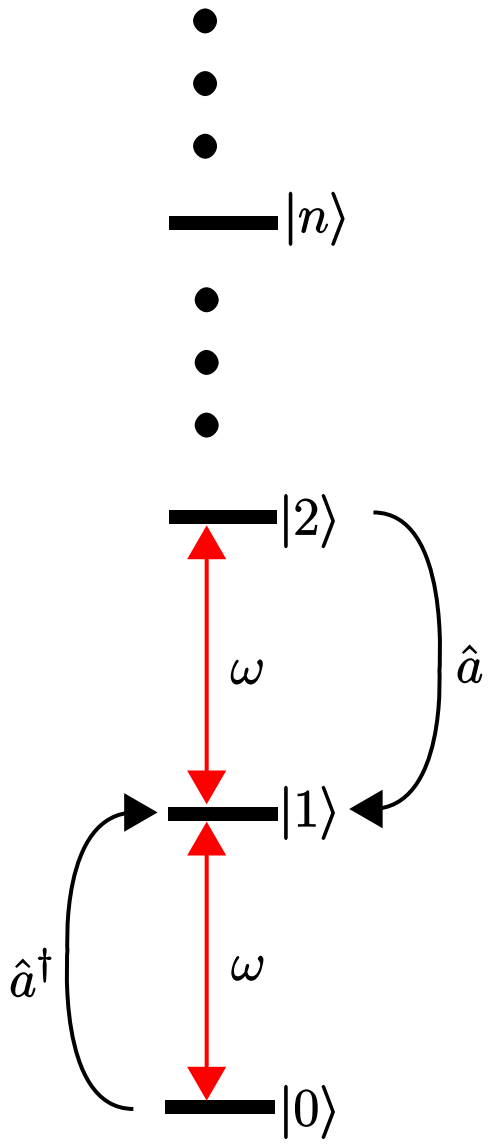

Figure 2.3: The quantum harmonic oscillator has infinitely many energy eigenstates, each separated in energy by $E = \hbar\omega$. The action of creation and annihilation operators are also shown.

We are interested in studying the behavior of quantum harmonic oscillators because a single mode of an optical cavity is perfectly described as a one dimensional quantum harmonic oscillator [30]. In this case, the frequency of the oscillator is given by the resonance frequency of the mode ω_c.

With a framework for both two–level atoms and optical cavity modes in place, the rest of this chapter will study the interaction between these systems coupled together.

2.4 Single atom: Jaynes–Cummings model

The Jaynes–Cummings model describes the behavior of a single two–level atom, which acts as a spin–$\frac{1}{2}$ system, coupled to a single mode of an optical cavity, which acts like a quantum harmonic oscillator (see Figure 2.4). The Hamiltonian that describes this system is given by:

$$\hat{H} = \hat{H}_a + \hat{H}_c + \hat{H}_{int} \tag{2.12}$$

where $\hat{H}_a = \hbar\omega_0\frac{\hat{\sigma}_Z}{2}$ is the spin–$\frac{1}{2}$ Hamiltonian of an atom with transition frequency ω_0, $\hat{H}_c = \hbar\omega_c\hat{c}^\dagger\hat{c}$ is the Hamiltonian of the cavity mode with resonant frequency ω_c, and $\hat{H}_{int} = -\hat{\mathbf{D}}\cdot\hat{\mathbf{E}}_c$ is the interaction Hamiltonian describing the interaction of the atomic dipole $\hat{\mathbf{D}}$ with the electric field $\hat{\mathbf{E}}_c$ inside the cavity. It can be shown that both the atomic dipole and cavity electric field can be written in terms of the raising and lowering operators introduced earlier, which along with the rotating wave approximation yields the following expression for the atom–cavity coupling term [31]:

$$\hat{H}_{int} = -\imath\hbar\frac{\Omega_0}{2}(\hat{c}\hat{\sigma}_+ - \hat{c}^\dagger\hat{\sigma}_-) \tag{2.13}$$

The two terms of this Hamiltonian correspond to absorption (where the atom absorbs a photon from the cavity mode and is raised to the excited state) and emission (where the atom emits a photon into the cavity mode and returns to the ground state). Here the 'vacuum Rabi frequency' Ω_0 has been defined as:

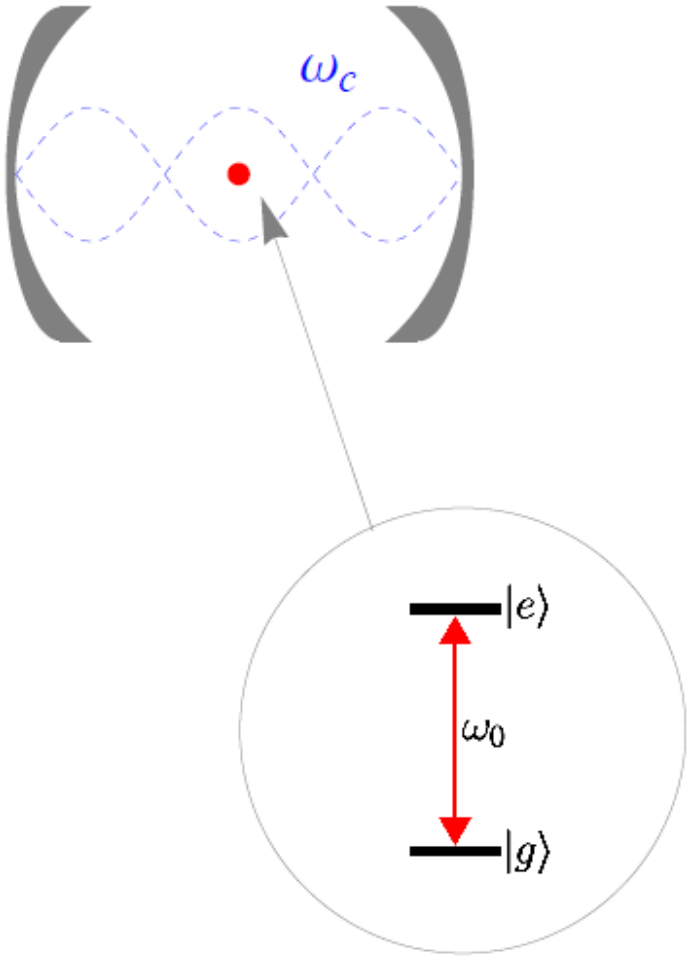

Figure 2.4: In the Jaynes–Cummings Hamiltonian, a two–level atom with resonance frequency ω_0 is coupled to an optical cavity mode with frequency ω_c (image adapted from Prince Max, 2013).

$$\Omega_0 \equiv 2\frac{d\varepsilon_0 \vec{\epsilon_a}^* \cdot \vec{\epsilon_c}}{\hbar} \tag{2.14}$$

where d is the dipole matrix element of the atomic transition, ε_0 is the amplitude of the electric field, and $\vec{\epsilon_a}/\vec{\epsilon_c}$ are the unit polarization vectors of the atomic transition and cavity mode respectively. The vacuum Rabi frequency is a critically important quantity in cavity QED physics, and describes the relative strength of the electric dipole interaction between the atom and the cavity field.

When the cavity mode and atomic transition are resonant ($\omega_0 = \omega_c$), the Hamiltonian takes a very simple form in the basis of states $|g, 1\rangle$ (atom in ground state, single photon in cavity) and $|e, 0\rangle$ (atom in excited state, zero photons in cavity) [31]:

$$\hat{H} = \frac{\hbar}{2}\begin{pmatrix} 0 & -\Omega_0 \\ \Omega_0 & 0 \end{pmatrix} \tag{2.15}$$

Since these two states are degenerate, perturbation theory requires diagonalizing the Hamiltonian to find the new eigenstates and eigenenergies of the system. The two 'dressed states' are given by:

$$|\pm\rangle = \frac{1}{\sqrt{2}}(|e, 0\rangle \pm \imath\, |g, 1\rangle) \tag{2.16}$$

with eigenenergies $E_\pm = \pm\hbar\Omega_0/2$. This is an important result, and the energy level diagram showing this process is in Figure 2.5. The other important result to notice is that there are two dressed modes as a result of coupling between two quantum systems: the atom and the cavity. In the last section of this chapter two distinct atomic modes and the cavity mode create three dressed states.

2.5 Many atoms: Tavis–Cummings model

The Tavis–Cummings model describes the interaction of an ensemble of N atoms with a single cavity mode. Written in the rotating frame of the atomic transition $|g\rangle \rightarrow |e\rangle$ at transition

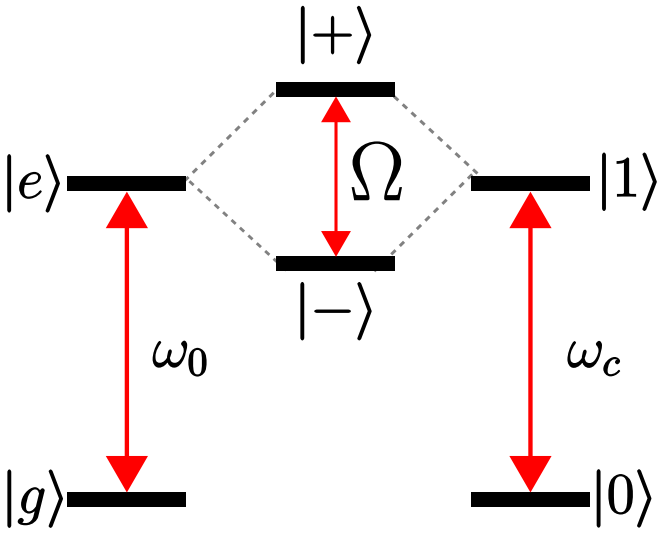

Figure 2.5: When an atomic transition frequency ω_0 becomes equal to a cavity resonance frequency ω_c, two nondegenerate dressed states $|\pm\rangle$ are formed which are split in frequency by Ω.

frequency ω_0, the Hamiltonian is given by [32]:

$$\hat{H} = \hbar\delta_c \hat{c}^\dagger \hat{c} + \hbar g(\hat{J}_- \hat{c}^\dagger + \hat{J}_+ \hat{c}) \tag{2.17}$$

where $\delta_c = \omega_c - \omega_0$ is the detuning of the cavity from atomic resonance and $g = \langle \hat{\mathbf{d}} \cdot \hat{\mathbf{E}} \rangle / \hbar$ is the coupling strength between an individual atom and the cavity mode. This Hamiltonian bears a striking resemblance to equation 2.12, but with the single–atom raising and lowering operators replaced by collective raising and lowering operators $\hat{J}_\pm = \sum_i \hat{\sigma}_{i\pm}$.

As before, the first term in the Hamiltonian describes the number of photons stored in the cavity. The second term describes both processes of photon emission from the atoms into the cavity mode and the reverse process: absorption of photons from the cavity mode by the atoms. The atom populations in the ground and excited states are given by the collective projection operators $\hat{N}_g = \sum_i |g_i\rangle \langle g_i|$ and $\hat{N}_e = \sum_i |g_e\rangle \langle g_e|$. The expectation values of these projection operators are denoted by $N_g \equiv \langle \hat{N}_g \rangle$ and $N_e \equiv \langle \hat{N}_e \rangle$ as shorthand.

The coupled atom–cavity system is probed by driving the system with incident light. If the system is only weakly driven, such that most of the atoms remain in the ground state ($N_e/N_g \ll 1$, $N_g \approx N$), the ensemble of atoms (each an individual spin–$\frac{1}{2}$ system) acts like a quantum harmonic oscillator with frequency ω_0. This is the limit of the Holstein–Primakoff approximation [33], which replaces the collective atomic raising and lowering operators with effective creation and annihilation operators: $\hat{a}^\dagger \approx \hat{J}_+/\sqrt{N}$ and $\hat{a} \approx \hat{J}_-/\sqrt{N}$. The approximation fails as a significant portion of the atoms are excited, since saturation effects begin to occur (i.e. an ensemble of N atoms can hold at most N excitations). With this approximation, the Hamiltonian becomes:

$$\hat{H} = \hbar\delta_c \hat{c}^\dagger \hat{c} + \hbar\sqrt{N} g(\hat{a}\hat{c}^\dagger + \hat{a}^\dagger \hat{c}) \tag{2.18}$$

which describes two coupled quantum harmonic oscillators. This Hamiltonian shows that the coupling between the atomic mode and the cavity mode is proportional to the square root of the number of atoms in the system. The collective Rabi frequency (in contrast to the single atom Rabi

frequency of equation 2.14) is defined as:

$$\Omega \equiv \sqrt{N} 2g \tag{2.19}$$

Tavis–Cummings Hamiltonian dynamics are very similar to the Jaynes–Cummings Hamiltonian, where the two dressed states are again separated in energy by $\hbar\Omega$. For example, the measured energy spacing between the two dressed states has been used to nondestructively measure the number of atoms in a cavity [34].

The dynamics of the system can be determined using the Heisenberg picture, which describe the time evolution of operators (as opposed to the Schrodinger picture where the operators remain constant in time and the state vectors evolve instead):

$$\frac{d}{dt}\hat{A}(t) = \frac{\imath}{\hbar}[\hat{H}, \hat{A}(t)] \tag{2.20}$$

for any operator $\hat{A}$ and Hamiltonian $\hat{H}$. Using the commutation relations $[\hat{c}, \hat{c}^\dagger] = [\hat{a}, \hat{a}^\dagger] = 1$ and $[\hat{a}, \hat{c}] = 0$, it can be shown that the Heisenberg equations of motion for the Jaynes–Cummings Hamiltonian in equation 2.18 are given by:

$$\dot{c} = -\imath\delta_c c - \imath\sqrt{N} g a \tag{2.21}$$

$$\dot{a} = -\imath\sqrt{N} g c \tag{2.22}$$

where the complex variables $a \equiv \langle\hat{a}\rangle$ and $c \equiv \langle\hat{c}\rangle$ are the expectation values of bosonic lowering operators describing the collective excitation of the atoms a and the cavity c. In the Holstein–Primakoff approximation, the number of excitations in the atoms and the cavity mode is given by $M_a = |a|^2$ and $M_c = |c|^2$ respectively.

The time evolution operator $e^{-\imath\hat{H}t/\hbar}$ is unitary, indicating that probability and energy are conserved (i.e. energy is stored either in the cavity or the atoms). Damping processes, as a result of cavity loss and spontaneous emission of the atoms, requires a Lindblad master equation approach

using the density matrix formalism [31]. The density matrix is a more general representation of a quantum state vector because it can describe mixed states (statistical ensembles of pure states). With nonunitary damping and drive terms, the Heisenberg equations of motion (2.22) become:

$$\dot{c} = -(\imath\delta_c + \frac{\kappa}{2})c - \imath\sqrt{N}ga + \sqrt{\kappa_1}c_i e^{\imath\delta_p t} \tag{2.23}$$

$$\dot{a} = \frac{\gamma}{2}a - \imath\sqrt{N}gc \tag{2.24}$$

for cavity linewidth κ and spontaneous emission rate γ of the atomic transition. The second term in equation 2.24 describes a driving field with complex amplitude c_i where κ_1 is the coupling of the input cavity mirror. The driving field has probe frequency ω_p and is detuned from atomic resonance by $\delta_p = \omega_p - \omega_0$.

The two normal modes of the atom–cavity system have eigenfrequencies $\omega_\pm$ given by [32]:

$$\omega_\pm = \frac{\delta_c \pm \sqrt{\delta_c^2 + \Omega^2}}{2} \tag{2.25}$$

and linewidths $\kappa'_\pm$ given by:

$$\kappa'_\pm = \frac{\kappa + (\frac{\Omega}{2\omega_\pm})^2\gamma}{1 + (\frac{\Omega}{2\omega_\pm})^2} \tag{2.26}$$

When the cavity is on resonance with the atomic transition ($\delta_c = 0$), the total frequency splitting is equal to the collective vacuum Rabi splitting ($\omega_+ - \omega_- = \Omega$) as expected. Observation of vacuum Rabi splitting indicates that the quantum system is in the strongly coupled regime, and is a hallmark feature of modern cavity QED experiments. Quantum nondemolition measurements can be performed by measuring the vacuum Rabi splitting, which can be used in applications like spin–squeezing and nondestructive atom counting [35, 36].

2.6 Two atomic transitions

We can generalize the Heisenberg equations of motion (2.24) to a three–level atom with two excited states by introducing a second atomic mode, denoted b. In our system specifically, the two

atomic modes are the $m_j = \pm 1$ Zeeman sublevels of an atomic transition. To describe this new system, we can extend the linearized input-output equations of [32] to include an additional atomic transition written in a rotating frame at the average atomic transition frequency ω_0 as:

$$\dot{a} = -\frac{1}{2}(\gamma + \imath\Delta)\, a - \imath\frac{1}{2\sqrt{2}}\Omega\, c \tag{2.27}$$

$$\dot{b} = -\frac{1}{2}(\gamma - \imath\Delta)\, b - \imath\frac{1}{2\sqrt{2}}\Omega\, c \tag{2.28}$$

$$\dot{c} = -\frac{1}{2}(\kappa + \imath 2\delta_c)\, c - \imath\frac{1}{2\sqrt{2}}\Omega\,(a+b) + \sqrt{\kappa_1}c_i e^{\imath\delta_p t}. \tag{2.29}$$

where ω_0 is now the average atomic transition frequency, and the two atomic transitions are separated in energy by $\hbar\Delta$. Here, $\delta_c = \omega_c - \omega_0$ is the detuning of the cavity resonance frequency ω_c from the average atomic resonance frequency and Ω is the observed collective vacuum Rabi splitting when $\Delta = 0$. Again γ is the decay rate of the excited atomic states, κ is the cavity power decay rate, and κ_1 is the coupling of the input cavity mirror that is driven by an externally incident probe field with complex amplitude c_i and at a probe frequency ω_p and detuning from average atomic resonance $\delta_p = \omega_p - \omega_0$ (see Figure 2.6).

The complex field transmitted through the cavity is $c_t = \sqrt{\kappa_2}c$ with κ_2 the coupling of the output mirror. The transmitted probe power relative to incident probe power is $P_T = |c_t/c_i|^2$ and the relative phase is $\psi = \arg(c_t/c_i)$. We can look for the steady state solutions to the input driving field c_i by imposing that $c_i = |c_i|e^{\imath\delta_p t}$ and $\frac{d|c_i|}{dt} = 0$. Under these conditions, we can analytically solve the system of equations for a, b, and c.

Figure 2.7 shows a simulation of the transmitted power and phase of this system. Rather than two dressed modes, as in the Tavis–Cummings model discussed earlier, we can see that the spectrum of the new atom–cavity system shows three resonances.

The work of this thesis is focused on studying the behavior of the central resonant feature, which is near resonance with the cavity. The full expression for transmitted power through the central feature is given by:

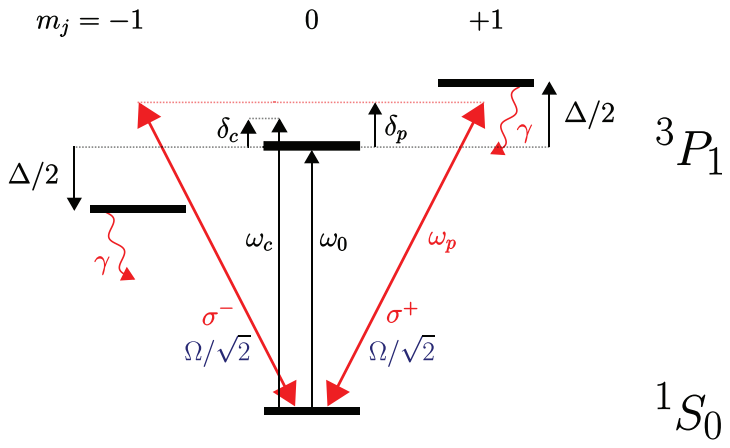

Figure 2.6: Energy level diagram. The Zeeman sublevels ($m_j = 0, \pm 1$) of the ^{1}S$_0$ to ^{3}P$_1$ atomic transition are split in energy by $\hbar\Delta$ with an applied dc magnetic field. Each transition spontaneously decays into free space at rate γ. The cavity resonant frequency is in general detuned by $\delta_c = \omega_c - \omega_0$, where ω_0 is the $m_j = 0$ transition frequency. Horizontally polarized probe light with detuning $\delta_p = \omega_p - \omega_0$ can be decomposed into circularly polarized $\sigma^\pm$ light, which couples to the $m_j = \pm 1$ states with Rabi frequency $\Omega/\sqrt{2}$, but not the $m_j = 0$ state.

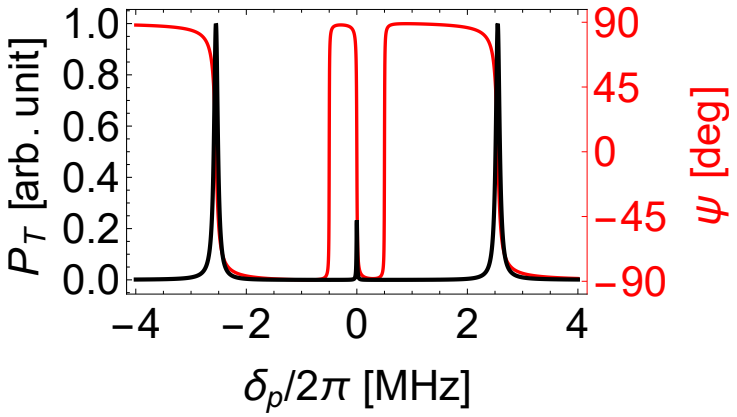

Figure 2.7: Linearized theory showing the power P_T and phase ψ of the transmitted probe light, plotted here for $\Omega/2\pi = 5$ MHz, $\Delta/2\pi = 1$ MHz, $\gamma/2\pi = 7.5$ kHz, and $\kappa/2\pi = 160$ kHz. Transmitted power has been normalized to the peak power of the two outer resonances.

$$P_T = 4\kappa_1 \left| \frac{(\gamma + 2\imath\delta_p)^2 + \Delta^2}{((\gamma + 2\imath\delta_p)^2 + \Delta^2)(2(\delta_c + \delta_p) - \imath\kappa) + (2\delta_p - \imath\gamma)\Omega^2} \right|^2 \tag{2.30}$$

with the relative phase of the transmitted light given by:

$$\psi = \arg \frac{-\imath(\Delta^2 + (\gamma + 2\imath\delta_p)^2)\kappa_1}{(\Delta^2 + (\gamma + 2\imath\delta_p)^2)(2\delta_p - \imath\kappa) + (2(\delta_c + \delta_p) - \imath\gamma)\Omega^2} \tag{2.31}$$

When the cavity and probe laser are on resonance with the average atomic transition frequency ($\delta_c = \delta_p = 0$), the transmitted probe power of this central mode is given by the simpler expression:

$$P_T = \frac{4(\gamma^2 + \Delta^2)^2\kappa_1}{((\gamma^2 + \Delta^2)\kappa + \gamma\Omega^2)^2} \tag{2.32}$$

For $\delta_c = 0$, the relative phase of the transmitted light becomes:

$$\psi = \arg \frac{-\imath(\Delta^2 + (\gamma + 2\imath\delta_p)^2)\kappa_1}{(\Delta^2 + (\gamma + 2\imath\delta_p)^2)(2\delta_p - \imath\kappa) + (2\delta_p - \imath\gamma)\Omega^2} \tag{2.33}$$

The amplitude and phase response of the central resonance feature can also be viewed in IQ plots, as a combination of in-phase (I) and quadrature (Q) components. Figure 2.8 shows IQ plots of light transmitted through the central feature while the cavity is on resonance ($\delta_c = 0$) for several different values of Zeeman splitting. Figure 2.9 shows the transmitted power and phase as a function of probe detuning for the same Zeeman splittings.

Important quantities about this central resonance feature relevant to frequency stabilization of lasers, such as linewidth and pulling coefficient, can be derived from these transmitted power and phase expressions. These quantities are experimentally measured and compared to theoretical predictions in Chapter 4 and discussed in Chapter 5.

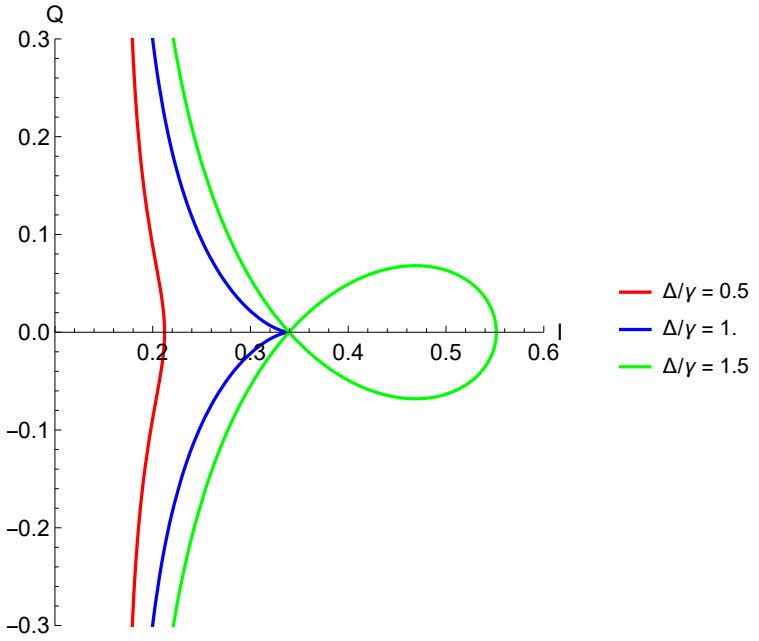

Figure 2.8: IQ response of the central resonance feature, parametrically plotted as a function of δ_p between ± 50 kHz for three different Zeeman splittings: $\Delta/\gamma = 0.5$ (red trace), $\Delta/\gamma = 1$ (orange trace), and $\Delta/\gamma = 1.5$ (green trace). The other parameters used are $\gamma = 7.5$ kHz, $\kappa = 2\kappa_1 = 160$ kHz, $\Omega = 5$ MHz, and $\delta_c = 0$, which are typical experimental values. The characteristic behavior of the resonance changes as Δ approaches γ.

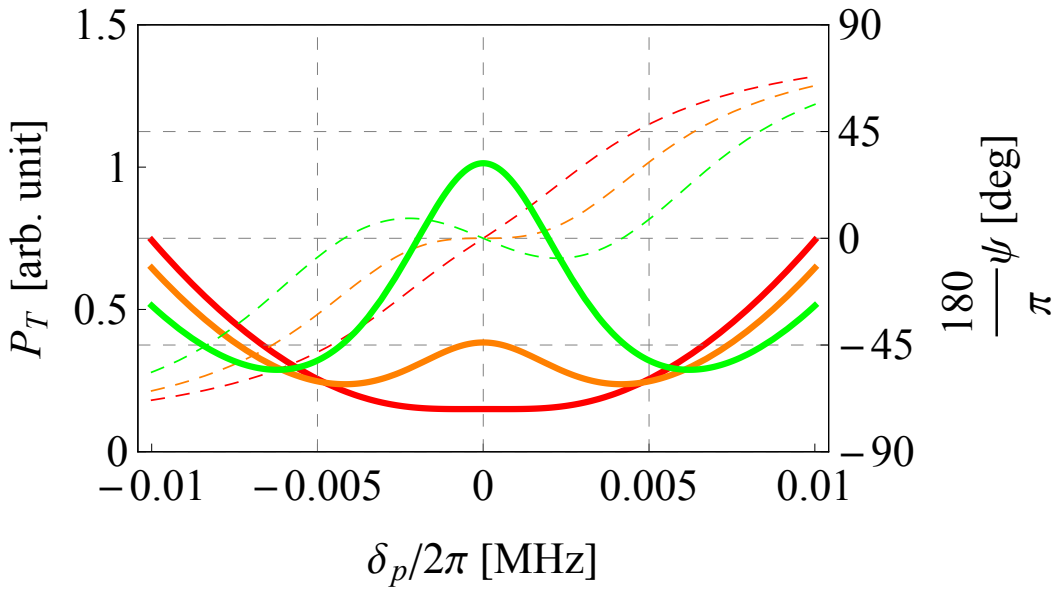

Figure 2.9: Power P_T (solid lines) and phase ψ (dashed lines) of light transmitted through the central resonance feature for three different Zeeman splittings: $\Delta/\gamma = 0.5$ (red trace), $\Delta/\gamma = 1$ (orange trace), and $\Delta/\gamma = 1.5$ (green trace). The other parameters used are $\gamma = 7.5$ kHz, $\kappa = 2\kappa_1 = 160$ kHz, $\Omega = 5$ MHz, and $\delta_c = 0$.

Chapter 3

Experimental Methods

3.1 System

The experimental system consists of an optical cavity coupled to an ensemble of atoms (Figure 3.1). The optical cavity is made of two concave mirrors fixed to a macor (machineable glass ceramic) spacer (Figure 3.2). Both mirrors are attached to piezoelectric transducers, which allows the cavity resonance frequency ω_c to be arbitrarily tuned with a control signal (by changing the mirror spacing). The cavity has a measured power decay rate of $\kappa/2\pi = 150.3(4)$ kHz, which is determined by mirror loses and reflection/transmission coefficients, along with the cavity length.

Up to $N = 1.3 \times 10^6$ ^{88}Sr atoms are loaded into the cavity during each experiment. The spin forbidden $^1S_0$ to $^3P_1$ atomic transition (with wavelength $\lambda_0 = 689$ nm) is used, which spontaneously decays into free space at rate $\gamma/2\pi = 7.5$ kHz.

Atoms are coupled to a single TEM00 mode of the cavity at collective vacuum Rabi frequency $\Omega = \sqrt{N}2g$, where $2g = 15$ kHz is the rms single–atom Rabi frequency found by averaging over the standing–wave cavity mode. [1]

Further details on atom preparation and confinement in the optical cavity are given in the following section.

[1] In reality the atoms are inhomogeneously coupled to the cavity mode since the 813nm optical lattice spacing is different than the 689nm standing wave of the TEM00 cavity mode.

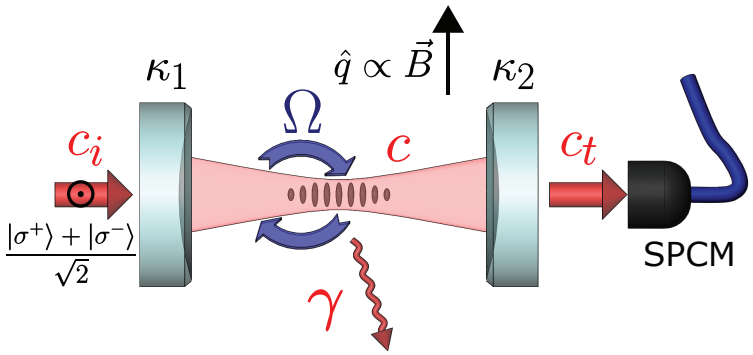

Figure 3.1: Experimental diagram. Atoms (red dots) spontaneously decay from the excited state at rate $\gamma/2\pi = 7.5$ kHz. The optical cavity has power decay rate $\kappa = \kappa_1 + \kappa_2$. Atoms are coupled to the cavity mode with collective Rabi frequency Ω. Horizontally polarized probe light can be decomposed into circular $\sigma^{\pm}$ components which interact with Zeeman sublevels which are split out by the applied magnetic field $\vec{B}$. The incident probe light field is c_i, and the field inside the cavity is c. The transmitted field c_t is collected with an SPCM (single photon counting module).

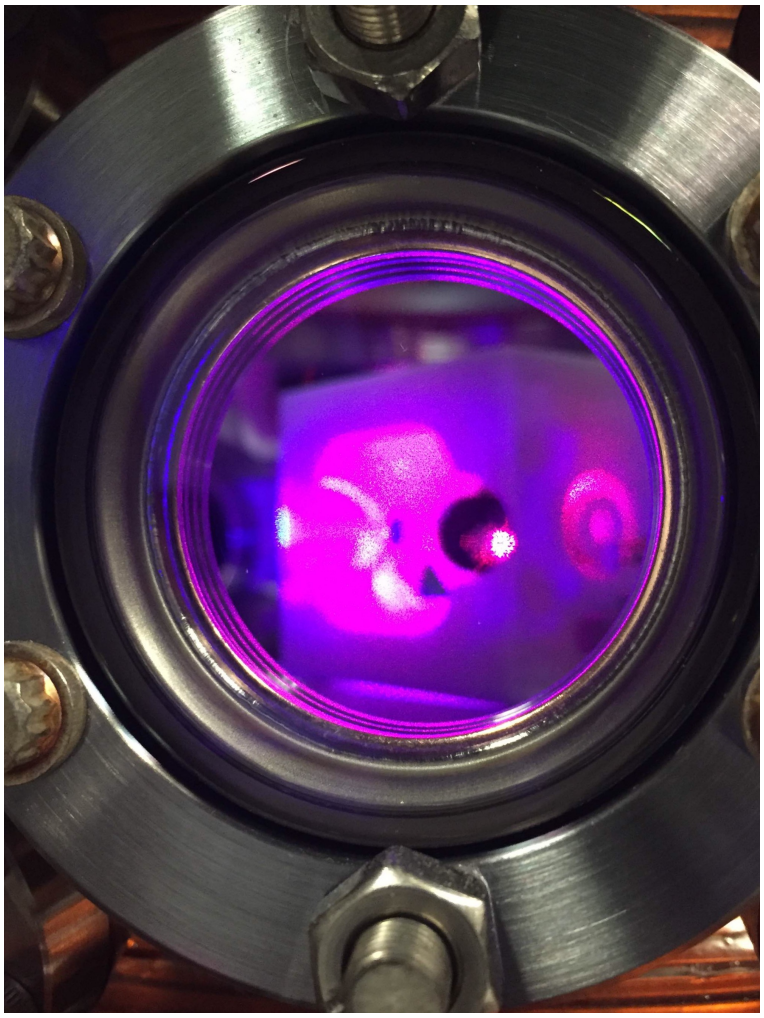

Figure 3.2: Picture of vacuum chamber and macor cavity spacer as seen through a viewport on the chamber. For scale, the cavity spacer is ~ 2 cm. External MOT coils used to generate the trapping magnetic field can also be seen outside the chamber.

3.2 Atom preparation

Atoms are cooled and trapped in the cavity using a variety of standard AMO techniques. First, a beam of hot atoms is created from a solid chunk of strontium using an oven. The beam is then longitudinally cooled using a Zeeman slower, and transversely cooled using a pair of 2D MOTs (magneto–optical traps). The atoms are then trapped and cooled in the main chamber using a two–stage MOT sequence. Finally the atoms are loaded into an optical lattice trap, where they collectively interact with the optical cavity.

3.3 Measurements

The system is probed using a laser coupled to the cavity. The transmitted power of the probe beam is measured using an SPCM (single photon counting module). In the experiment we sweep the frequency of the probe laser in order to find the resonant frequencies of dressed modes, which appear as transmission peaks on the SPCM. In order to generate this frequency sweep, the probe laser is first modulated with an electro–optic modulator (EOM), creating sidebands. One of these sidebands is used to probe the transmission of the atom–cavity system. By tuning the rf modulation frequency of the EOM, we are able to arbitrarily move the probe laser sideband over the frequency range of interest.

3.4 Experiment Parameters

Table 3.1 gives a summary the actual parameter values used in the experiment.

Table 3.1: Experiment parameters

Experiment parameter	**Numerical value**
Atomic transition free space decay rate γ	$2\pi \times 7.5$kHz
Atomic transition wavelength λ_0	689nm
Total atom number N	$\sim 1.3 \times 10^6$
Lattice trap depth	100(10) μK
Final atom temperature	10(1) μK
Cavity power decay rate $\kappa = \kappa_1 + \kappa_2$	$2\pi \times 150$kHz
Single–atom vacuum Rabi splitting frequency $2g$	15kHz
Single–atom cooperativity parameter $C = \frac{4g^2}{\kappa\gamma}$	0.2
Zeeman frequency splitting per Gauss Δ	(2.1MHz/G)

Chapter 4

Results and Discussion

This chapter details the experimental results of probing the atom–cavity system described in Chapter 3. We first demonstrate a collective Rabi splitting with no applied magnetic field, which indicates that our experiment is in the strongly coupled regime ($\Omega \gg \kappa, \gamma$). This is the system described by the Tavis–Cummings Hamiltonian, where the resonant atomic and cavity modes interfere to create two new dressed states: one at higher energy and one at lower energy. We then apply an external magnetic field to split the degenerate sublevels of the atomic transition.

4.1 MIT transmission spectrum

As discussed in Chapter 3, the coupled atom-cavity system is interrogated using a probe laser. After interacting with the atom–cavity system, the transmitted probe light is collected onto an SPCM (recall Figure 3.1).

Figure 4.1 shows the full transmission spectrum as a function of probe laser detuning δ_p and Zeeman splitting Δ, for the cavity on resonance with the average atomic transition frequency ($\delta_c = 0$). In order to generate the data in this figure we linearly sweep the probe laser's frequency over the atom–cavity resonances and record a time–trace of the power transmitted to the SPCM. We repeat this measurement for different Zeeman splittings by adjusting the strength of the applied magnetic field. The red trace at $\Delta = 0$ displays an ordinary collective vacuum Rabi splitting $\Omega/2\pi = 5(1)$ MHz, which results from the coupling between the ensemble of atoms and the cavity mode. However, a new third resonance appears at the cavity resonance frequency as the Zeeman

sublevels are split out by the applied magnetic field. We refer to this resonance as the "dark state" resonance since it disappears when the magnetic field is turned off.

This transmission spectrum suggests that the dark state resonance has both atom–like and cavity–like properties. At very large Zeeman splittings ($\Delta \gg \Omega, \gamma$), the dark state mode is the only visible resonance of the atom–cavity system, since the other two modes have been Zeeman–shifted far away from the cavity resonance. In fact, the transmission spectrum in this regime is identical to that of a bare cavity. This is the case because the two atomic modes have been so far detuned from the cavity mode by the applied magnetic field that there is virtually no coupling between the atoms and the cavity (in other words, the probe light which is being transmitted by the cavity is far off resonance from both atomic transitions). This is the "cavity–like" regime. In the opposite limit where the Zeeman splitting is very small ($\Delta \ll \Omega, \gamma$), the dark state resonance completely decouples from the probe light. In this case any probe light that is resonant with the cavity mode and would normally be transmitted is instead absorbed and scattered by the atoms into free space, so no light is transmitted through the cavity mode at all. This is the "atom–like" regime.

With these two limiting behaviors in mind, we introduce a mixing angle θ which quantifies the relative atom–like and cavity–like behavior of the dark state. The mixing angle is defined by:

$$\sin^2\theta = \frac{\bar{\Delta}^2}{\Omega^2 + \bar{\Delta}^2} \tag{4.1}$$

where the effective detuning $\bar{\Delta}$ is defined as $\bar{\Delta}^2 = \Delta^2 + \gamma^2$.

The character of the dark state excitation is given by the ratio of the probability that the excitation is photonic-like $P_c = M_c/(M_c + M_a + M_b) = \sin^2\theta$ versus atomic-like $P_{ab} = (M_a + M_b)/(M_c + M_a + M_b) = \cos^2\theta$. The dark state excitation can decay into free space at rate R_{ab} or by emission through the cavity mirrors R_c, with the ratio of the rates given simply by $R_{ab}/R_c = \gamma/(\kappa \tan^2\theta) = NC(\gamma/\bar{\Delta})^2$.

The rest of this chapter focuses on studying the new dark state mode. We measure both the linewidth and pulling coefficient of the dark state. Both measurements are consistent with the atom–

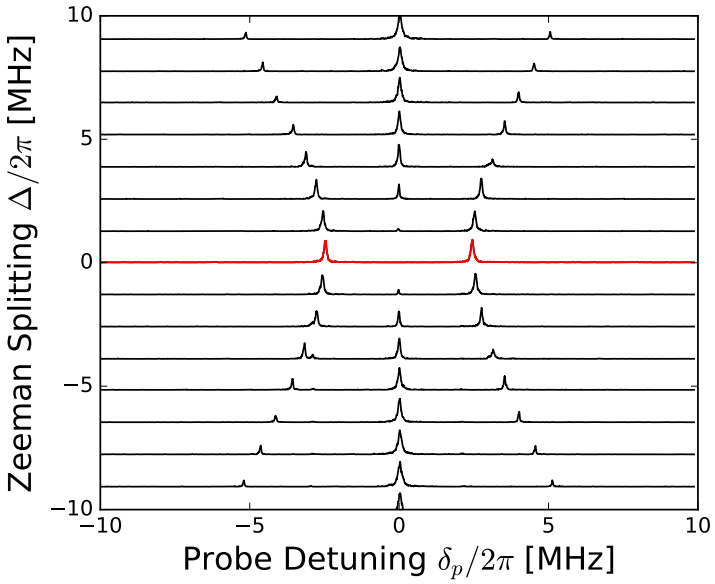

Figure 4.1: Full MIT transmission spectrum. The transmitted power through the cavity versus the probe detuning δ_p, with $\delta_c = 0$. Each trace was taken for different applied magnetic fields, creating different Zeeman splittings Δ labeled on the vertical. The central red trace is taken for $\Delta = 0$ and displays a collective vacuum Rabi splitting $\Omega/2\pi = 5(1)$ MHz. When a magnetic field is applied perpendicular to the probe polarization, inducing a Zeeman splitting Δ, a new transmission feature appears in between the two original resonances of the vacuum Rabi splitting.

like and cavity–like behavior demonstrated in the full transmission spectrum shown previously.

4.2 Effective linewidth measurements

The linewidth of any frequency resonance is an important attribute for laser stabilization and precision measurement applications, as a laser stabilized to a narrow spectroscopic feature is less sensitive to technical offsets than a laser stabilized to a broader feature. We can calculate the effective linewidth κ' of any spectroscopic feature by determining how quickly the phase changes $\delta\psi$ as the probe frequency changes: $d\psi/dt = \delta_p/(\kappa'/2)$. The full expression for the linewidth of the dark state resonance is given by:

$$\kappa' = \frac{(\gamma^2 + \Delta^2)((\gamma^2 + \Delta^2)\kappa + \gamma\Omega^2)}{(\gamma^2 + \Delta^2)^2 + (-\gamma^2 + \Delta^2)\Omega^2} \tag{4.2}$$

Written using the newly defined mixing angle, the effective linewidth is given by:

$$\kappa' = (\gamma \cos^2\theta + \kappa \sin^2\theta)/b \tag{4.3}$$

The term in parentheses is a weighted average of atom and cavity linewidths that reflects the character of the mode. The correction factor is $b = d\cos^2\theta + \sin^2\theta$, where $d = (\Delta^2 - \gamma^2)/\bar{\Delta}^2$. When $\Delta \gg \gamma$, both b and d approach unity. At small detunings $\Delta \sim \gamma$, the responses of the dark and bright modes to the applied drive become comparable, causing a modification of the correction factor. Figure 4.2 shows a logarithmic plot of the effective linewidth as a function of Zeeman splitting. In the regime experimentally explored with this work ($b \approx 1$), κ' is simply the full width at half maximum linewidth of the power transmission feature. For $\Omega \gg \Delta \gg \gamma$, the mixing angle is small and the linewidth approaches the atomic linewidth $\kappa' \approx \gamma$ (atom–like regime), which can be much narrower than the cavity linewidth κ. In the opposite limit of $\Delta \gg \Omega \gg \gamma$, the effective linewidth approaches the bare cavity linewidth $\kappa' \approx \kappa$ (cavity–like regime).

The effective linewidth of the dark state mode can be measured from the MIT transmission spectra in Figure 4.1 by fitting a Lorentzian function to the dark state resonance of each trace,

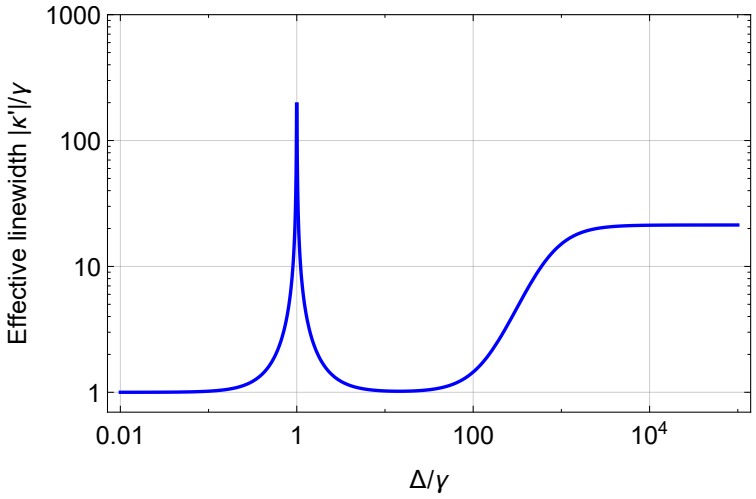

Figure 4.2: Theoretically predicted effective linewidth magnitude $|\kappa'|$ of dark state resonance as a function of Zeeman splitting Δ. κ' changes sign near $\Delta = \gamma$ due to the correction factor b (equation 4.3). Parameters used are $\gamma = 7.5$ kHz, $\kappa = 2\kappa_1 = 160$ kHz, $\Omega = 5$ MHz, and $\delta_c = 0$.

and then extracting the full width at half maximum (FWHM) of the Lorentzian. The results of this analysis are shown in Figure 4.3 for several collective vacuum Rabi frequencies. We are able to calculate the effective linewidth for different collective vacuum Rabi frequencies by varying the atom number.

In the atom–like regime, we can see that the effective linewidth approaches the atomic transition linewidth (lower dashed line), while in the cavity–like regime the effective linewidth reaches the cavity linewidth (upper dashed line) as expected. We can also observe that for larger vacuum Rabi frequencies, the dark state mode retains its atom–like behavior for larger Zeeman splittings. This makes sense intuitively: the mode will behave more atom–like when a larger number of atoms are in the system.

4.3 Relative transmission measurements

In addition to extracting the effective linewidth from the MIT transmission spectrum, it is also informative to measure the peak transmission of the dark mode resonance. As discussed previously in section 4.1 we expect the relative transmission of the dark state mode to disappear in the atom–like regime since the atoms will absorb and scatter any resonant probe light into free space, while in the cavity–like regime maximum transmission should occur since the atoms will not be resonant with the probe light. The maximum transmitted power P_{max} calculated earlier in Chapter 2 can be rewritten using the mixing angle as:

$$P_{max} = \frac{4\kappa_1\kappa_2}{\kappa^2}\frac{1}{\left(1+\frac{\gamma}{\kappa\tan^2\theta}\right)^2}. \tag{4.4}$$

We can check this formula by looking at the behavior in both the atom–like and cavity–like regimes: As the Zeeman splitting decreases, $\tan^2\theta$ and P_{max} go to zero as expected. In the opposite limit of large Zeeman splitting, the maximum transmission approaches that of an empty cavity $P_{max} \to P_{empty} = 4\kappa_1\kappa_2/\kappa^2$. A logarithmic plot of the transmitted power through the dark state resonance is shown in Figure 4.4

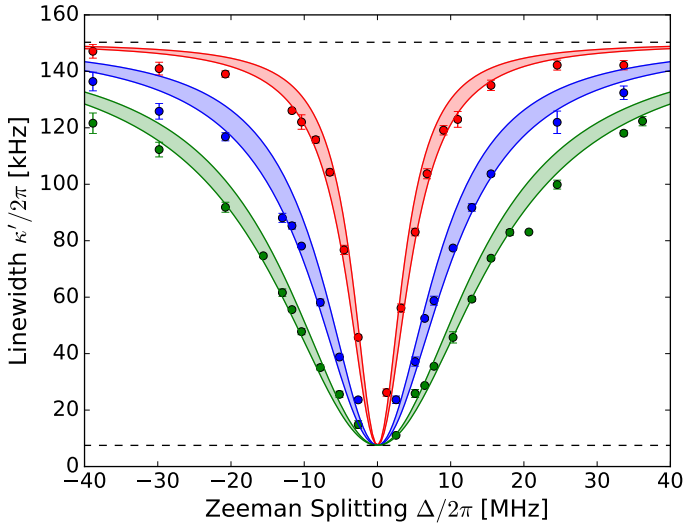

Figure 4.3: Measured linewidth of the central MIT transmission feature versus the induced Zeeman splitting between excited states. The traces are taken for three different collective vacuum Rabi frequencies $\Omega/2\pi = 4.6(5)$ (red), 10(1) (blue), and 16(1) (green) MHz, with values set by changing the total atom number N. The upper dashed line is the empty cavity's linewidth κ, and the lower dashed line is the atomic transition's linewidth γ. The minimum observed linewidth was 11 kHz. The shaded regions are no-free parameter predictions from the linearized model introduced in the text, indicating the ± 1 standard deviation uncertainty bands based on independent measurements of Ω.

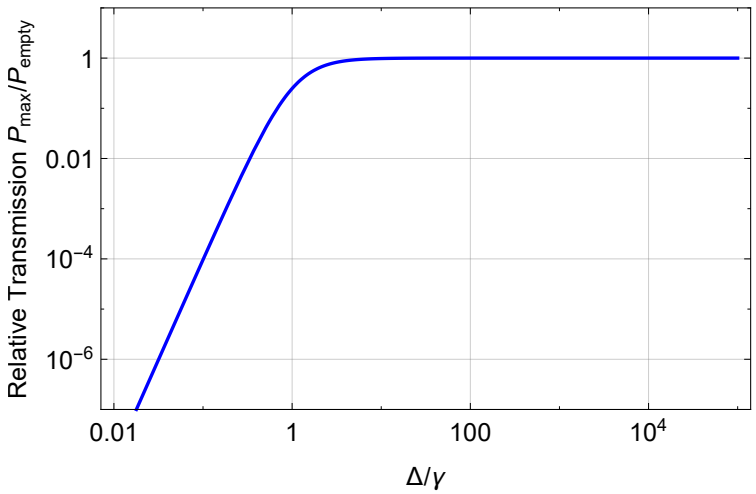

Figure 4.4: Theoretically predicted power transmission through the dark state resonance as a function of Zeeman splitting. Parameters used are $\gamma = 7.5$ kHz, $\kappa = 2\kappa_1 = 160$ kHz, $\Omega = 5$ MHz, and $\delta_c = 0$.

The peak transmission can be found by recording the maximum voltage of the SPCM for each probe laser frequency sweep. These results are shown in Figure 4.5.

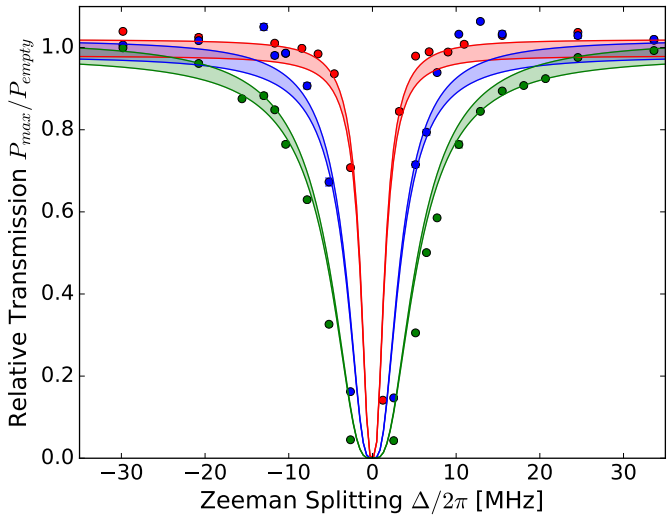

Figure 4.5: The measured peak transmitted power of the central MIT transmission feature for the same collective Rabi frequencies. Here, the transmitted power is normalized to the peak transmitted power when the cavity is empty. Again traces are taken for three different collective vacuum Rabi frequencies $\Omega/2\pi = 4.6(5)$ (red), 10(1) (blue), and 16(1) (green) MHz. The shaded regions indicate the ± 1 standard deviation uncertainty bands for the predictions.

The transmitted power of the dark state mode shows the expected atom–like and cavity–like behavior. Again, the dark state mode remains atom–like at larger Zeeman splittings when more atoms are in the system.

4.4 Pulling coefficient measurements

The pulling coefficient P is a measure of how much the dark state resonant frequency changes when the cavity mode resonant frequency is changed. It is defined as $P = \Delta\omega_D/\Delta\omega_c$, where $\Delta\omega_c$ is the change in cavity frequency and $\Delta\omega_D$ is the resulting change in dark state resonance frequency. A small pulling coefficient $P \ll 1$ is desirable for a frequency reference as it will be less sensitive to thermal fluctuations and technical noise on the reference cavity, which currently limit state-of-the-art lasers. The pulling coefficient can be rewritten using the mixing angle as:

$$P = \frac{\sin^2\theta}{b} \tag{4.5}$$

which is simply the cavity–like fraction of the dark state mode in the typical regime of operation ($b \approx 1$). A logarithmic plot of the pulling coefficient as a function of Zeeman splitting is shown in Figure 4.6.

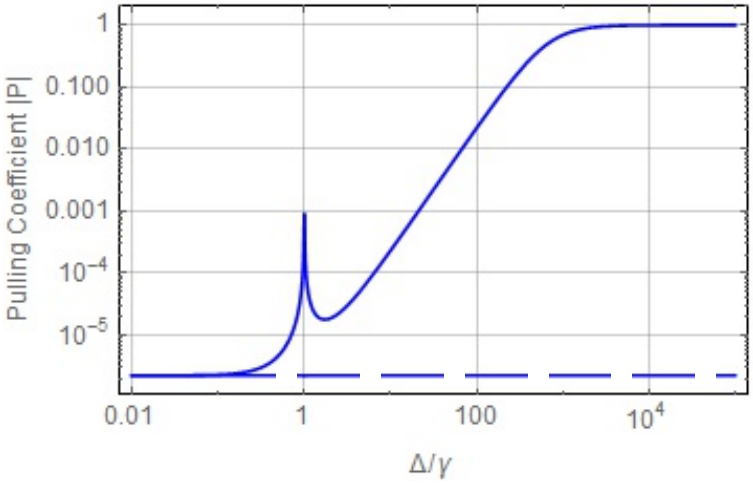

Figure 4.6: Theoretically predicted pulling coefficient magnitude $|P|$ of dark state mode versus Zeeman splitting Δ. The pulling coefficient switches signs near $\Delta = \gamma$ due to the correction factor b (equation 4.5). The lower dashed line is $\frac{\kappa}{\gamma}\frac{1}{NC}$, which is the minimum value of the pulling coefficient. Parameters used are $\gamma = 7.5$ kHz, $\kappa = 2\kappa_1 = 160$ kHz, $\Omega = 5$ MHz, $NC = 2.1 \times 10^4$, and $\delta_c = 0$.

We measured the pulling coefficient of the dark state by sweeping the probe laser frequency across resonance and fitting the center frequency ω_D with a Lorentzian. This is repeated while toggling ω_c between two values separated by 100 kHz. The results of this experiment are shown in Figure 4.7 for three different vacuum Rabi frequencies.

Again we observe that the dark state mode behaves atom–like for $\Delta \ll \Omega, \gamma$, where the pulling coefficient approaches zero and indicates that the mode is completely insensitive to the cavity. In the opposite limit the pulling coefficient approaches unity as the dark state becomes increasingly cavity–like. As the atom number increases the dark state again remains atom–like for larger Zeeman splittings.

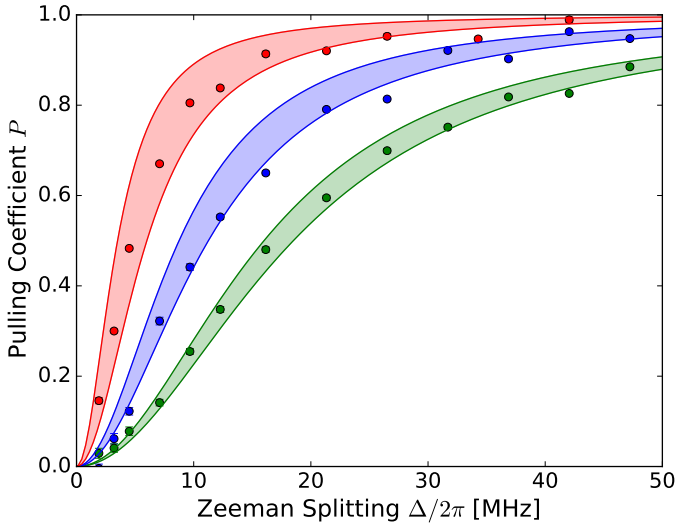

Figure 4.7: The pulling coefficient P versus Zeeman splitting Δ for several collective vacuum Rabi frequencies $\Omega/2\pi = 5(1)$ (red), $10(1)$ (blue), and $17(1)$ (green) MHz. The prediction from the linearized theory is shown with ± 1 standard deviation bands.

Chapter 5

Conclusions

In this thesis I have described the generation of a narrow spectroscopic feature using MIT. The feature was experimentally shown to be relatively insensitive to reference cavity fluctuations which limit state-of-the-art laser stability, with a minimum pulling coefficient P measured below 0.05. The feature also approaches the relatively narrow linewidth of the 7.5 kHz atomic transition.

The optimal parameter regime for using MIT in frequency reference applications requires balancing several parameters. For example, it is desired for a frequency reference to have a narrow linewidth and a small pulling coefficient (by reducing the Zeeman splitting Δ in our experiment), however this also reduces the transparency of the system which reduces signal-to-noise and requires more probe light to resolve. Increasing the probe light power is problematic because the light heats up the atoms via free–space scattering, which reduces atom number. Atom saturation effects can also occur if the probe light power is increased too much, where the Holstein–Primakoff approximation is no longer valid. Specific system requirements are needed to determine the optimal parameters of the MIT generated frequency reference.

While the majority of this work was done with the atoms trapped in the Lamb-Dicke regime (i.e. confined to much less than the wavelength of the probe light) with respect to the cavity axis, we have also performed scans of the cavity transmission spectrum in which the atoms were unconfined along the cavity axis. In this configuration, the rms Doppler shift along the cavity axis is roughly 45 kHz. Despite this inhomogeneous broadening, the center feature has a linewidth of 18.5 kHz, which is probably limited by technical noise on the cavity frequency that arises when the lattice

depth is reduced to release the atoms. The linewidth of the dark feature is most likely insensitive to inhomogeneous broadening so long as Δ is much larger than the inhomogeneous broadening [37]. This insensitivity to Doppler broadening may make such techniques suitable to continuously operating atomic beam experiments, where confining the atoms to the Lamb-Dicke regime would be challenging.

Bibliography

[1] Ambler Thompson and Barry N. Taylor. Guide for the Use of the International System of Units (SI). NIST Special Publication, 2008.

[2] T Kessler, C Hagemann, C Grebing, T Legero, U Sterr, F Riehle, MJ Martin, L Chen, and J Ye. A sub-40-mhz-linewidth laser based on a silicon single-crystal optical cavity. Nature Photonics, 6(10):687–692, 2012.

[3] BJ Bloom, TL Nicholson, JR Williams, SL Campbell, M Bishof, X Zhang, W Zhang, SL Bromley, and J Ye. An optical lattice clock with accuracy and stability at the 10-18 level. Nature, 506(7486):71–75, 2014.

[4] N Hinkley, JA Sherman, NB Phillips, M Schioppo, ND Lemke, K Beloy, M Pizzocaro, CW Oates, and AD Ludlow. An atomic clock with 10–18 instability. Science, 341(6151):1215–1218, 2013.

[5] Ichiro Ushijima, Masao Takamoto, Manoj Das, Takuya Ohkubo, and Hidetoshi Katori. Cryogenic optical lattice clocks. Nature Photonics, 9(3):185–189, 2015.

[6] Chin-Wen Chou, DB Hume, Till Rosenband, and DJ Wineland. Optical clocks and relativity. Science, 329(5999):1630–1633, 2010.

[7] Till Rosenband, DB Hume, PO Schmidt, CW Chou, A Brusch, L Lorini, WH Oskay, RE Drullinger, TM Fortier, JE Stalnaker, et al. Frequency ratio of al+ and hg+ single-ion optical clocks; metrology at the 17th decimal place. Science, 319(5871):1808–1812, 2008.

[8] Shimon Kolkowitz, Igor Pikovski, Nicholas Langellier, Mikhail D Lukin, Ronald L Walsworth, and Jun Ye. Gravitational wave detection with optical lattice atomic clocks. arXiv preprint arXiv:1606.01859, 2016.

[9] Peter W Graham, Jason M Hogan, Mark A Kasevich, and Surjeet Rajendran. New method for gravitational wave detection with atomic sensors. Physical review letters, 110(17):171102, 2013.

[10] Andrei Derevianko and Maxim Pospelov. Hunting for topological dark matter with atomic clocks. Nature Physics, 10(12):933–936, 2014.

[11] S Blatt, AD Ludlow, GK Campbell, Jan Westenkær Thomsen, T Zelevinsky, MM Boyd, J Ye, X Baillard, M Fouché, R Le Targat, et al. New limits on coupling of fundamental constants to gravity using sr 87 optical lattice clocks. Physical Review Letters, 100(14):140801, 2008.

[12] M. Bishof L. Jiang A. S. Sørensen J. Ye M. D. Lukin P. Komar, E. M. Kessler. A quantum network of clocks. Nature Physics, 10:582–587, May 2014.

[13] Kenji Numata, Amy Kemery, and Jordan Camp. Thermal-noise limit in the frequency stabilization of lasers with rigid cavities. Phys. Rev. Lett., 93(25):250602, Dec 2004.

[14] M. J. Martin, D. Meiser, J. W. Thomsen, Jun Ye, and M. J. Holland. Extreme nonlinear response of ultranarrow optical transitions in cavity qed for laser stabilization. Phys. Rev. A, 84:063813, Dec 2011.

[15] Philip G. Westergaard, Bjarke T. R. Christensen, David Tieri, Rastin Matin, John Cooper, Murray Holland, Jun Ye, and Jan W. Thomsen. Observation of motion-dependent nonlinear dispersion with narrow-linewidth atoms in an optical cavity. Phys. Rev. Lett., 114:093002, Mar 2015.

[16] Bjarke T. R. Christensen, Martin R. Henriksen, Stefan A. Schäffer, Philip G. Westergaard, David Tieri, Jun Ye, Murray J. Holland, and Jan W. Thomsen. Nonlinear spectroscopy of sr atoms in an optical cavity for laser stabilization. Phys. Rev. A, 92:053820, Nov 2015.

[17] Justin G Bohnet, Zilong Chen, Joshua M Weiner, Dominic Meiser, Murray J Holland, and James K Thompson. A steady-state superradiant laser with less than one intracavity photon. Nature, 484(7392):78–81, 2012.

[18] Matthew A. Norcia and James K. Thompson. Cold-strontium laser in the superradiant crossover regime. Phys. Rev. X, 6:011025, Mar 2016.

[19] Matthew A. Norcia, Matthew N. Winchester, Julia R. K. Cline, and James K. Thompson. Superradiance on the millihertz linewidth strontium clock transition. Science Advances, 2:10, 2016.

[20] D. Meiser, Jun Ye, D. R. Carlson, and M. J. Holland. Prospects for a millihertz-linewidth laser. Phys. Rev. Lett., 102(16):163601–163604, Apr 2009.

[21] K-J Boller, A Imamoğlu, and Stephen E Harris. Observation of electromagnetically induced transparency. Physical Review Letters, 66(20):2593, 1991.

[22] Martin Mücke, Eden Figueroa, Joerg Bochmann, Carolin Hahn, Karim Murr, Stephan Ritter, Celso J Villas-Boas, and Gerhard Rempe. Electromagnetically induced transparency with single atoms in a cavity. Nature, 465(7299):755–758, 2010.

[23] Gessler Hernandez, Jiepeng Zhang, and Yifu Zhu. Vacuum rabi splitting and intracavity dark state in a cavity-atom system. Physical Review A, 76(5):053814, 2007.

[24] Lene Vestergaard Hau, Stephen E Harris, Zachary Dutton, and Cyrus H Behroozi. Light speed reduction to 17 metres per second in an ultracold atomic gas. Nature, 397(6720):594–598, 1999.

[25] Chien Liu, Zachary Dutton, Cyrus H Behroozi, and Lene Vestergaard Hau. Observation of coherent optical information storage in an atomic medium using halted light pulses. Nature, 409(6819):490–493, 2001.

[26] R Zhao, YO Dudin, SD Jenkins, CJ Campbell, DN Matsukevich, TAB Kennedy, and A Kuzmich. Long-lived quantum memory. Nature Physics, 5(2):100–104, 2009.

[27] Thibault Peyronel, Ofer Firstenberg, Qi-Yu Liang, Sebastian Hofferberth, Alexey V Gorshkov, Thomas Pohl, Mikhail D Lukin, and Vladan Vuletić. Quantum nonlinear optics with single photons enabled by strongly interacting atoms. Nature, 488(7409):57–60, 2012.

[28] YO Dudin and A Kuzmich. Strongly interacting rydberg excitations of a cold atomic gas. Science, 336(6083):887–889, 2012.

[29] Jia Ningyuan, Alexandros Georgakopoulos, Albert Ryou, Nathan Schine, Ariel Sommer, and Jonathan Simon. Observation and characterization of cavity rydberg polaritons. Physical Review A, 93(4):041802, 2016.

[30] Claude N. Cohen-Tannoudji. Manipulating atoms with photons. Reviews of Modern Physics, 70:707–720, July 1998.

[31] Serge Haroche and Jean Michel Raimond. Exploring the Quantum: Atoms, Cavities, and Photons. Oxford Univ. Press, Oxford, 2006.

[32] Zilong Chen, Justin G. Bohnet, Joshua M. Weiner, Kevin C. Cox, and James K. Thompson. Cavity-aided nondemolition measurements for atom counting and spin squeezing. Phys. Rev. A, 89:043837, Apr 2014.

[33] T. Holstein and H. Primakoff. Field dependence of the intrinsic domain magnetization of a ferromagnet. Phys. Rev., 58:1098–1113, Dec 1940.

[34] Matthew A. Norcia and James K. Thompson. Strong coupling on a forbidden transition in strontium and nondestructive atom counting. Phys. Rev. A, 93:023804, Feb 2016.

[35] Zilong Chen, Justin G. Bohnet, Shannon R. Sankar, Jiayan Dai, and James K. Thompson. Conditional spin squeezing of a large ensemble via the vacuum Rabi splitting. Phys. Rev. Lett., 106:133601, Mar 2011.

[36] Matthew A. Norcia and James K. Thompson. Strong coupling on a forbidden transition in strontium and nondestructive atom counting. Phys. Rev. A, 93:023804, Feb 2016.

[37] R. Houdré, R. P. Stanley, and M. Ilegems. Vacuum-field Rabi splitting in the presence of inhomogeneous broadening: Resolution of a homogeneous linewidth in an inhomogeneously broadened system. Phys. Rev. A, 53:2711–2715, Apr 1996.